



INPAINTING WITH FOKKER-PLANCK EQUATION

Anca IGNAT

”Alexandru Ioan Cuza” University of Iași, Faculty of Computer Science
General Berthelot 16, Iași 700483, Romania

Corresponding author: Anca IGNAT, E-mail: ancai@info.uaic.ro

Abstract: In the present paper we employ the Fokker-Planck equation for completing an image with missing information. Using this equation has three advantages. The first one is the fact that this equation has a mild solution. The second advantage is that the implicit approximation scheme provides a sequence of solutions which converges to the solution of the Fokker-Planck equation. The third quality of this equation is the low regularization effect on the initial data, thus preserving the edges from the inpainted image. The numerical experiments show that this equation provides a good solution for the inpainting problem.

Key words: Fokker-Planck equation, implicit scheme, image inpainting

1. INTRODUCTION

Inpainting is the process of filling in missing parts from an image. It deals with the problem of coherently completing a damaged image, taking into account the surroundings of the absent/omitted regions. It is an interpolation problem that can be addressed using discrete or continuous methods. The discrete methods are using patch matching and/or sparse representation [1–3]. The continuous methods employ variational formulations or partial differential equations (p.d.e.) [4–6]. Very good surveys on image inpainting techniques can be found in [7, 8].

In the exemplar based approach, the missing information is filled in pixel by pixel, pixels that are placed on the border between the regions with and without information. The regions without information are completed by using patches from the image that suit best to the surroundings of the pixel to be inpainted.

In the p.d.e. approach the inpainted image is the solution of a conveniently chosen p.d.e or optimal control problem [6, 9–11]. Methods that use p.d.e. for image restoration or noise reduction can also be adapted for image inpainting [12].

Usually, the partial differential equation have a (strong) regularization effect on the starting data, producing regular solutions even if the initial data are not so smooth. From the image processing point of view this regularization process means losing edge information, producing blurred images.

In this paper we use the Fokker-Planck equation [13, 14] in order to fill the missing parts of a damaged image. The Fokker-Planck equation is a second-order, non-linear, parabolic p.d.e. that has a diffusion and a transport term. This equation has its origin in statistical physics, but it has also many applications in other domains as stochastic analysis, stochastic optimal control. We chose this equation because it has several advantages for the inpainting process. The first one is the fact that it is a well-posed problem. This equation has a weak/mild solution, it can be shown that the discrete, implicit approximation scheme’s solutions (weakly) converge to the Fokker-Planck solution. This mild solution is also one of the possible solutions of the inpainting problem, providing an image with filled in information. This convergence property is seldom addressed in inpainting methods that use p.d.e. Another advantage/benefit in using the Fokker-Planck equation is provided by the fact that it does not have a strong regularization effect, thus preserving the edge information of the image.

2. FOKKER-PLANCK EQUATION FOR IMAGE INPAINTING

For the inpainting problem we use the following Fokker-Planck equation:

$$\begin{aligned} \frac{\partial u}{\partial t} - \sum_{i,j=1}^2 \frac{\partial^2}{\partial x_i \partial x_j} (a_{ij}(x,u)u) + \operatorname{div}(b(x,u)u) &= 0 \quad \text{for } x \in \mathbb{R}^2, t > 0 \\ u(0,x) &= u_0(x) \quad x \in \mathbb{R}^2 \end{aligned} \quad (1)$$

where $b(x,u) = (b_1(x,u), b_2(x,u))$. The rectangular region $\Omega \subseteq \mathbb{R}^2$ represents the image, $\mathbb{R}^2 \setminus \Omega$ is the background and $u_0(x)$ is the damaged image. We denote by $u^*(x)$ the original image, the image with complete information. Starting from the damaged image $u_0(x)$, the purpose is to find an image $\tilde{u}(x)$ visually as close as possible to u^* . We assume that u^* and, consequently, u_0 are not affected by noise.

We can write the domain Ω as a reunion of two disjoint regions $\Omega = \Omega_i \cup \Omega_m$, $\Omega_i \cap \Omega_m = \emptyset$, such that:

$$u_0(x) = \begin{cases} u^*(x) & \text{for } x \in \Omega_i \\ 0 & \text{for } x \in \Omega_m \end{cases} \quad (2)$$

(Ω_m is the region of the image with missing information).

We assume that the functions $b, a_{ij} : \mathbb{R}^2 \times \mathbb{R}_+ \rightarrow \mathbb{R}$, $i, j = 1, 2$ satisfy the following conditions:

(i) $a_{ij} \in C^1(\mathbb{R}^2 \times \mathbb{R}) \cap C_b(\mathbb{R}^2 \times \mathbb{R})$, $\frac{\partial a_{ij}}{\partial x_k} \in C_b(\mathbb{R}^2 \times \mathbb{R})$, $\forall i, j, k = 1, 2$, $a_{12} = a_{21}$;

(ii) there exists a positive constant $\gamma > 0$ such that

$$\sum_{i,j=1,2}^2 (a_{ij}(x,u) + u \frac{\partial a_{ij}}{\partial u}(x,u)) \xi_i \xi_j \geq \gamma |\xi|^2, \quad \forall \xi \in \mathbb{R}^2, x \in \mathbb{R}^2, u \in \mathbb{R}; \quad (3)$$

(iii) $b_i \in C_b(\mathbb{R}^2 \times \mathbb{R})$.

We have denoted by C_b the space of continuous, bounded functions and by C^1 the space of continuous differentiable functions.

As regards existence for equation (1) we note the following result established in [13].

THEOREM 2.1. *Assume hypotheses (i)-(iii) are true. Then, for each $u_0 \in L^1(\mathbb{R}^2)$, there exists a unique solution $u = u(\cdot, u_0) \in C([0, \infty); L^1(\mathbb{R}^2))$ to equation (1). This solution u has the following properties:*

$$\|u(t, u_0^1) - u(t, u_0^2)\|_1 \leq \|u_0^1 - u_0^2\|_1, \quad \forall u_0^1, u_0^2 \in L^1(\mathbb{R}^2), t \geq 0, \quad (4)$$

$$u \geq 0 \text{ a.e. in } (0, +\infty) \times \mathbb{R}^2 \text{ if } u_0 \geq 0 \text{ a.e. in } \mathbb{R}^2 \quad (5)$$

$$\int_{\mathbb{R}^2} u(t, x) dx = \int_{\mathbb{R}^2} u_0(x) dx, \quad \forall u_0 \in L^1(\mathbb{R}^2), t \geq 0, \quad (6)$$

and u is a solution of (1) in the sense of Schwartz distributions on $[0, \infty) \times \mathbb{R}^2$, that is:

$$\int_0^\infty \int_{\mathbb{R}^2} \left(u(t,x) \varphi_t(t,x) + \sum_{i,j=1}^2 a_{ij}(x, u(t,x)) u(t,x) \frac{\partial^2 \varphi(t,x)}{\partial x_i \partial x_j} + \right. \quad (7)$$

$$\left. + b(x,u) \cdot \nabla_x \varphi(t,x) u(t,x) \right) dt dx = 0, \quad \forall \varphi \in C^\infty((0, \infty) \times \mathbb{R}^2).$$

Here $\|\cdot\|_1$ is the norm of $L^1(\mathbb{R}^2)$.

The proof of this theorem relies on Crandall–Liggett existence result for non-linear Cauchy problems of the following form:

$$\begin{aligned} \frac{du}{dt} + Au &= 0 \quad , \quad t \geq 0, \\ u(0) &= u_0 \in X \end{aligned} \quad (8)$$

in a Banach space X , with the norm $\|\cdot\|$, where the nonlinear operator $A : D(A) \subseteq X \rightarrow X$ is m -accretive, i.e., for each $\lambda > 0$, $R(I + \lambda A) = X$ and:

$$\|(I + \lambda A)^{-1}u - (I + \lambda A)^{-1}v\| \leq \|u - v\| \quad \forall u, v \in X, \lambda > 0. \quad (9)$$

A mild solution for equation (8) is a continuous function $u : [0, +\infty) \rightarrow X$ that satisfies, for each $0 < T < \infty$, the following relations:

(a) $u(x) = \lim_{h \rightarrow 0} u_h(t)$ strongly in X , uniformly in $t \in [0, T]$, where $u_h : [0, T] \rightarrow X$ is defined by:

$$(b) \quad u_h(t) = u_h^i, \quad t \in [ih, (i+1)h], \quad i = 0, 1, \dots, N, \quad N = \left\lceil \frac{T}{h} \right\rceil$$

(c) the sequence u_h^i is obtained by solving the following equations:

$$(I + hA)u_h^{i+1} = u_h^i, \quad i = 0, \dots, N-1, \quad u_h^0 = u_0 \quad (10)$$

For the Fokker-Planck equation (1), the space $X = L^1(\mathbb{R}^2)$ and the operator A is given by:

$$\begin{aligned} Au &= - \sum_{i,j=1}^2 \frac{\partial^2}{\partial x_i \partial x_j} (a_{ij}(x, u)u) + \operatorname{div}(b(x, u)u) \quad \text{in } \mathcal{D}'(\mathbb{R}^2) \\ D(A) &= \{u \in L^1(\mathbb{R}^2); Au \in L^1(\mathbb{R}^2)\} \end{aligned} \quad (11)$$

Then, under assumption (9), for each initial data $u_0 \in \overline{D(A)}$ there is a unique mild solution $u \in C([0, T]; X)$ to equation (1) (see [15, p. 130]).

The finite difference scheme (b), (c) has in this case the following form:

$$\begin{aligned} u_h^{i+1} - h \sum_{k,j=1}^2 \frac{\partial^2}{\partial x_k \partial x_j} (a_{kj}(x, u_h^{i+1})u_h^{i+1}) + \\ + \operatorname{div}(b(x, u_h^{i+1})u_h^{i+1}) &= u_h^i \quad \text{in } \mathcal{D}'(\mathbb{R}^2) \\ u_h^0 &= u_0 \quad \text{in } \mathbb{R}^2. \end{aligned} \quad (12)$$

We have denoted by $\mathcal{D}'(\mathbb{R}^2)$ the space of Schwartz distributions on \mathbb{R}^2 .

As shown in [13], for all i , the solution $u_h^{i+1} \in L^1(\mathbb{R}^2)$ to the above equation (12) exists in sense of distributions; however, by elliptic regularizations it follows via bootstrap arguments that $u_h^{i+1} \in W_{\text{loc}}^{1,q}$ for some $q > 1$ if i is sufficiently large. Anyway, even for small values of i ($i = 0, 1$), u_h^{i+1} is more regular than the initial data u_0 .

3. NUMERICAL APPROXIMATIONS AND EXPERIMENTS

The existence of the weak solution to equation (1) guarantees that the discrete solution of the numerically approximated problem converges to this solution.

The implicit approximation scheme for the Fokker-Planck equation (1) is the following:

$$\begin{aligned} u^{t+1}(x) &= u^t + \delta_t A^h u^{t+1}(x), \quad x \in \bar{\Omega}, t = 0, 1, \dots, \delta_t < 1 \\ u^0(x) &= u_0(x), \quad x \in \bar{\Omega} \end{aligned} \quad (13)$$

where $\bar{\Omega} \subseteq \mathbb{R}^2$ is the discrete correspondent of domain Ω ,

$$\bar{\Omega} = \{(x_1^i, x_2^j); i = 1, M, j = 1, N\}$$

for a $N \times M$ digital image.

The operator A^h , $h = (h_1, h_2)$, is the discrete approximation of operator A (11) by using the following finite difference approximations for the partial derivatives:

$$\begin{aligned} \frac{\partial^2 g}{\partial x_1^2}(x_1, x_2) &\approx \frac{g(x_1 + h_1, x_2) - 2g(x_1, x_2) + g(x_1 - h_1, x_2)}{h_1^2} \\ \frac{\partial^2 g}{\partial x_2^2}(x_1, x_2) &\approx \frac{g(x_1, x_2 + h_2) - 2g(x_1, x_2) + g(x_1, x_2 - h_2)}{h_2^2} \\ \frac{\partial^2 g}{\partial x_1 x_2}(x_1, x_2) &\approx \frac{g(x_1 + h_1, x_2) - g(x_1 - h_1, x_2) + g(x_1, x_2 + h_2) - g(x_1, x_2 - h_2)}{2h_1 h_2} \\ \frac{\partial g}{\partial x_1}(x_1, x_2) &\approx \frac{g(x_1 + h_1, x_2) - g(x_1 - h_1, x_2)}{2h_1} \\ \frac{\partial g}{\partial x_2}(x_1, x_2) &\approx \frac{g(x_1, x_2 + h_2) - g(x_1, x_2 - h_2)}{2h_2}. \end{aligned} \quad (14)$$

In these numerical approximations we consider:

$$u^t(x) = 0 \quad \text{when } x \notin \bar{\Omega}, \forall t.$$

For $a_{ij}, i, j = 1, 2, b_i, i = 1, 2$ we used polynomial functions of the following form:

$$\begin{aligned} a_{ij}(x, u) &= a_{ij}(u) = \gamma + u^{p_{ij}}, \quad i, j = 1, 2, \quad p_{12} = p_{21} \\ b_i(x, u) &= w_1(\alpha + u^{q_i}), \quad i = 1, 2 \end{aligned} \quad (15)$$

with $p_{ij}, q_i \in [-0.5, 2]$.

In order to evaluate the quality of the inpainting process three classical estimators were employed: peak signal to noise ratio (PSNR), structural similarity (SSIM) and L^1 -norm:

$$\begin{aligned} \text{PSNR}(u, v) &= 10 \log_{10} \frac{L^2}{\text{MSE}(u, v)} \\ \text{MSE}(u, v) &= \frac{1}{MN} \sum_{i=0}^{M-1} \sum_{j=0}^{N-1} [u(x_1^i, x_2^j) - v(x_1^i, x_2^j)]^2 \\ \text{SSIM}(u, v) &= \frac{(2\mu_u \mu_v + c_1)(2\sigma_{uv}^2 + c_2)}{(\mu_u^2 + \mu_v^2 + c_1)(\sigma_u^2 + \sigma_v^2 + c_2)} \end{aligned} \quad (16)$$

where u and v are two digital images to be compared, L is the dynamical range (usually, for 8-bit images $L = 255$), $\mu_u, \mu_v, \sigma_u^2, \sigma_v^2, \sigma_{uv}^2$ are the expected values, variances and cross-variances of the two images, respectively.



Fig. 1 – Images to be inpainted.

In order to test this method, we use three images for inpainting, that can be seen in Fig. 1. Starting from the same shape, we build four small masks (50×50) with four orientations: horizontal, vertical, $\pm 45^\circ$ (see Fig. 2). We apply these small masks in a regular, grid like manner as in Fig. 3.

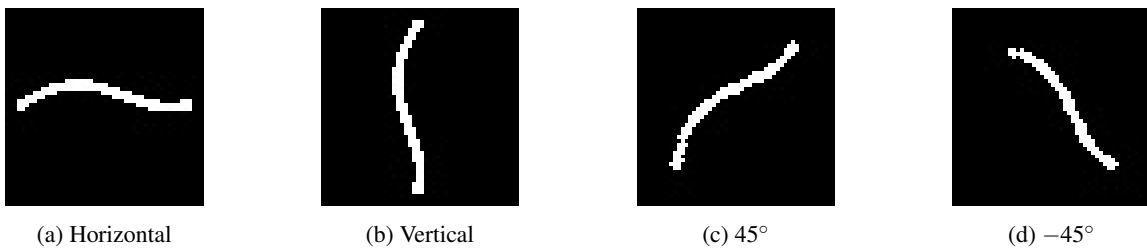


Fig. 2 – Small masks.

We performed 150 iterations with $\delta_t = 0.05$, without the transport term of (1) and obtain the results from Table 1 where we denoted by Im1 Botero's Mona Lisa, Im2 is the Siriu Lake image and Im3 is da Vinci's Mona Lisa. Note that for the portrait images the best results are for the diagonal masks and for the landscape the horizontal mask provided the best errors.

Table 1
Inpainting error results for small patches – without transport term

	L^1 -error			PSNR		
	Im1	Im2	Im3	Im1	Im2	Im3
Horizontal	74.9608	91.2995	74.502	43.4653	43.7074	46.7556
Vertical	65.0824	107.3804	77.8157	44.5495	42.4596	46.6387
45°	56.4275	104.2353	72.7608	46.5424	42.8236	47.3217
-45°	59.5137	102.1765	71.5804	46.064	42.4068	46.961

¹<https://images-na.ssl-images-amazon.com/images/I/51a3mOcIR%2BL.jpg>

²https://upload.wikimedia.org/wikipedia/commons/thumb/7/70/Siriu_Lake.jpg/1920px-Siriu_Lake.jpg

³https://upload.wikimedia.org/wikipedia/commons/e/ec/Mona_Lisa%2C_by_Leonardo_da_Vinci%2C_from_C2RMF_retouched.jpg

In order to test the influence of the shape of the missing part and the content of the image to be inpainted we used the same parameters on two small subimages from Botero's *Monalisa* (see Fig. 4). In these computations we also introduced the transport term. We used the Fokker-Planck equation with and without the transport term. The employed parameters are:

$$p = \begin{pmatrix} 0.8 & 1.5 \\ 1.5 & 1.3 \end{pmatrix}, \quad q = \begin{pmatrix} 0.8 \\ 0.8 \end{pmatrix}, \quad \alpha = \gamma = 0.01, \quad w_1 = 2.5 \quad (17)$$



Fig. 3 – Images with missing information.

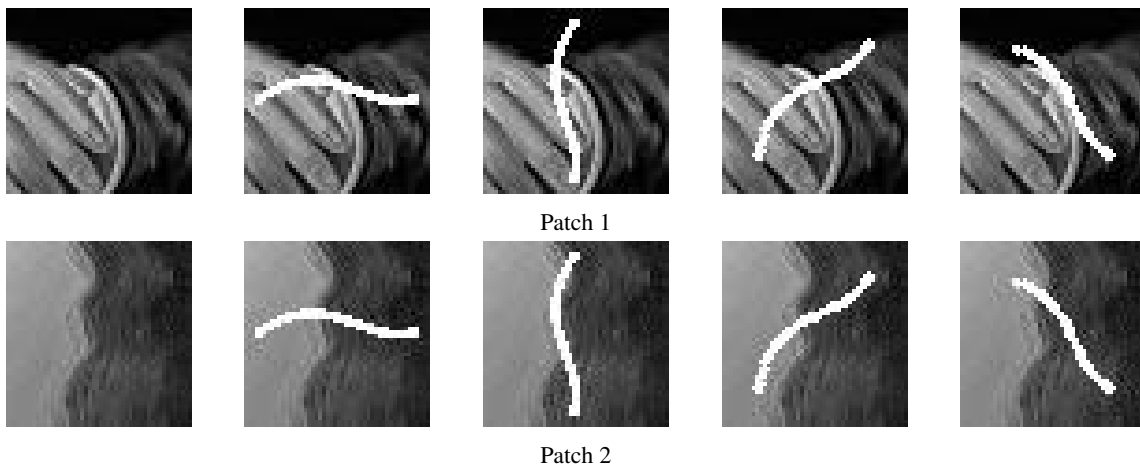


Fig. 4 – Subimages from Bortero's *Monalisa* (to be inpainted).

In Fig. 5 are some inpainted images using different masks.

In Table 2 are the results for the L^1 -norm and SSIM evaluators for inpainting without the transport term and in Table 3 are the results for the method using also the transport term. These results show that the inpainting procedure we propose is strongly influenced by the shape and orientation of the missing part and the content of the image to be inpainted.

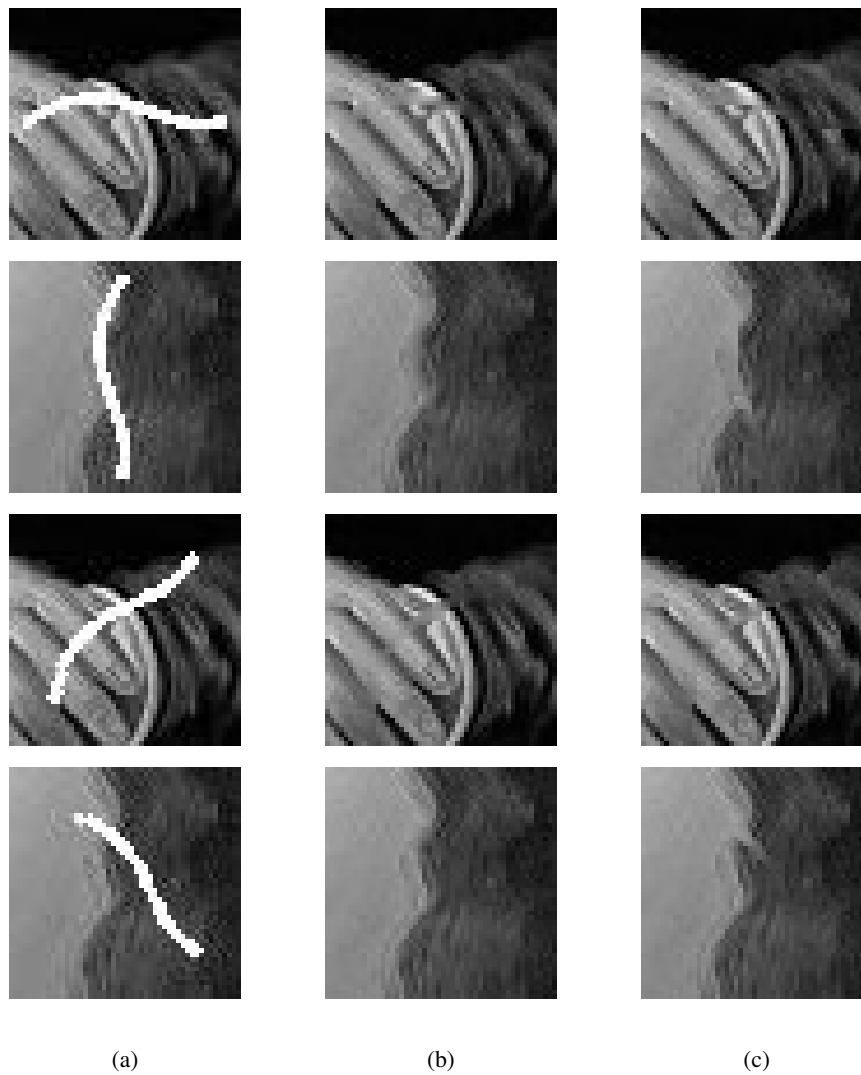


Fig. 5 – Inpainted subimages from Bortero’s Mona Lisa: a) patch with missing information; b) inpainted without transport term; c) inpainted with transport term.

Table 2
Inpainting error results for small patches – without transport term

	Patch 1		Patch 2	
	L^1 -error	SSIM	L^1 -error	SSIM
Horizontal	13.6016	97.7472	2.892	98.6697
Vertical	11.3729	97.7861	5.151	98.64
45°	8.28	98.6806	2.732	98.7883
-45°	16.3789	96.9242	2.5171	99.0878

Table 3
Inpainting error results for small patches – with transport term

	Patch 1		Patch 2	
	L^1 -error	SSIM	L^1 -error	SSIM
Horizontal	12.0833	98.0576	3.8518	98.0771
Vertical	10.6993	98.2388	6.3955	97.8867
45°	8.5845	98.3152	3.0625	98.5772
-45°	17.4326	96.1304	5.874	97.5897

From these computations it seems that the best results are obtained using the Fokker-Planck equation without the transport term. Although, other computations show that the inpainting process depends on the parameters we choose the functions involved in equation (1), so it is possible to obtain better results using other parameters. For example, for Patch 1 and mask -45° the parameters $q = (0.8, 0)$ and $w_1 = 1$ yield an L^1 -error of 12.1977 and SSIM 97.8936 which is better than the result obtain without transport term.

4. CONCLUSIONS

We presented in this paper a new method for image inpainting using a numerical approximation for the Fokker-Planck equation. The solution for the Fokker-Planck equation is computed as the mild limit of solutions for discrete implicit schemes associated to equation (1), thus providing a robust method for image inpainting. Numerical results show that this equation completes the missing parts of the images in a visually coherent manner. The inpainting process is influenced by the functions involved in Fokker-Planck equation, the shape of the missing part and the content of the image to be inpainted. It needs to be further studied how to choose these parameters in order to obtain results as good as possible.

REFERENCES

1. A. CRIMINISI, P. PÉREZ, K. TOYAMA, *Region filling and object removal by exemplar-based image inpainting*, IEEE Transactions on image processing, **13**, pp. 1200–1212, 2004.
2. J. WANG, K. LU, D. PAN, N. HE, B-k. BAO, *Robust object removal with an exemplar-based image inpainting approach*, Neurocomputing, **123**, pp. 150–155, 2014.
3. V. CASELLES, *Exemplar-based image inpainting and applications*, SIAM News, **44**, pp. 1–3, 2011.
4. M. BERTALMIO, G. SAPIRO, V. CASELLES, C. BALLESTER, *Image inpainting*, Proceedings of the 27th Annual Conference on Computer graphics and interactive techniques, ACM Press/Addison-Wesley Publishing Co., 2000, pp. 417–424.
5. W. CASACA, M. BOAVENTURA, M.C. DE ALMEIDA, L.G. NONATO, *Combining anisotropic diffusion, transport equation and texture synthesis for inpainting textured images*, Pattern Recognition Letters, **36**, pp. 36–45, 2014.
6. C-B. SCHÖNLIEB, *Partial differential equation methods for image inpainting*, vol. **29**, Cambridge University Press, 2015.
7. C. GUILLEMOT, O. LE MEUR, *Image inpainting: Overview and recent advances*, IEEE signal processing magazine, **31**, pp. 127–144, 2014.
8. M. BERTALMIO, V. CASELLES, S. MASNOU, G. SAPIRO, *Image inpainting*, Acta Metallurgica, <https://www.dtic.upf.edu/~mbertalmio/bertalmi.pdf>.
9. T. BARBU, *Second-order anisotropic diffusion-based framework for structural inpainting*, Proceedings of the Romanian Academy, Series A: Mathematics, Physics, Technical Sciences, Information Science, **19**, 2, pp. 329–336, 2018.
10. P. LI, S-J. LI, Z-A. YAO, Z-J. ZHANG, *Two anisotropic fourth-order partial differential equations for image inpainting*, IET Image Processing, **7**, pp. 260–269, 2013.

11. W. CASACA, M. BOAVENTURA, M. C. DE ALMEIDA, L.G. NONATO, *Combining anisotropic diffusion, transport equation and texture synthesis for inpainting textured images*, Pattern Recognition Letters, **36**, pp. 36–45, 2014.
12. T. BARBU, V. BARBU, *A PDE approach to image restoration problem with observation on a meager domain*, Nonlinear Analysis: Real World Applications, **13**, pp. 1206–1215, 2012.
13. V. BARBU, M. RÖCKNER, *From nonlinear Fokker-Planck equations to solutions of distribution dependent SDE*, arXiv preprint arXiv:1808.10706, 2018.
14. V. BARBU, *Generalized solutions to nonlinear Fokker-Planck equations*, Journal of Differential Equations, **261**, pp. 2446–2471, 2016.
15. V. BARBU, *Nonlinear differential equations of monotone types in Banach spaces*, Springer Science & Business Media, 2010.

Received on January 8, 2019